

Visible-Light-Driven Photocatalytic Degradation of Rhodamine B Using WO₃-based Particles

Nompumelelo Z. Mzimela*, Shepherd M. Tichapondwa, Evans M. N. Chirwa

Water Utilisation and Environmental Engineering Division, Department of Chemical Engineering,
 University of Pretoria, Pretoria 0002.
u11262835@tuks.co.za

Bioaccumulation of synthetic organic dyes in wastewater as a result of industrial effluents is a growing concern. These dyes are known to be resistant to conventional biological water treatment processes. This has compelled the search for more effective and sustainable water treatment procedures. This work investigates the use of visible light active WO₃-based photocatalysis as a possible technology for the removal of these dyes. Tungsten trioxide (WO₃) nanoparticles were synthesized via a facile chemical precipitation method. These particles were characterized using X-ray diffraction (XRD), scanning electron microscopy (SEM), scanning electron microscopy/energy dispersive x-ray spectroscopy (SEM/EDS), transmission electron microscopy (TEM) and Brunauer-Emmett-Teller (BET) to confirm the crystallinity, elemental composition, structural morphology, and specific surface area. X-ray diffraction characterization revealed that the nature of the material was biphasic (WO₃/WO₃·0.5H₂O). BET surface area analysis showed that upon calcination, the surface area increased from 0.1611 to 25.4 m²/g. Preliminary experiments showed that the degradation of Rhodamine B using WO₃-based particles was highly pH dependent, with rapid degradation occurring under alkaline conditions. A pH of 9.5 was chosen for this study. A 96.1 % degradation efficiency of Rhodamine B was achieved at an optimum catalyst loading of 5 g/L after 4 h of irradiation.

1. Introduction

The textile industry is one of the major contributors of water pollution which ultimately leads to water scarcity. Approximately 95 - 400 L of water is required to process a kilogram of textiles. According to a World Bank Report, the textile industry is reported to be responsible for 17- 20 % of industrial water pollution (Jiang et al., 2019). Rhodamine B, a cationic xanthene dye, is one of the most widely used dyes in the textile industry. The molecular structure of Rhodamine B (Figure 1) contains multiple aromatic rings making it highly stable and thus difficult to biodegrade (Tavakoli-Azar et al., 2020). Organic dyes have carcinogenic, mutagenic, and allergenic properties which renders them harmful to humans, microorganisms, and aquatic life. Traditional wastewater treatment methods which include ozonation, membrane filtration, bioadsorption, ion exchange removal, biological/ aerobic treatment, and coagulation (Rafiq et al., 2021) cannot completely degrade organic pollutants, as a result, semiconductor photocatalysis, an advanced oxidation process (AOP) has gained a lot of attention as a possible solution. Semiconductor photocatalysis is environmentally friendly, inexpensive and can completely degrade organic pollutants without producing secondary pollution. It is referred to as a 'green' technology in the treatment of pollutant infested wastewater (Adenuga et al., 2019). The mechanistic rationale behind photocatalysis is the generation of e⁻/h⁺ pairs within the photocatalyst which triggers the formation of highly reactive hydroxyl radicals which are involved in the mineralization of organic pollutants into H₂O and CO₂ (Rajput et al., 2022). The photoresponse of the semiconductor upon light irradiation is primarily dependent on the band gap energy of the particles and the intensity of the incident light (Scarsella et al., 2017). The application of photocatalysis is, however, restricted by knowledge gaps which include photocatalytic reactor design, mechanistic understanding of the interaction between pollutants and photocatalysts and tailoring morphologies of photocatalysts to achieve efficient pollutant removal (Zhang et al., 2019). It is anticipated that this work will address some of these research gaps. Prior research has mainly focused on the use of TiO₂ as a photocatalyst. However, due to its wide bandgap of 3.2 eV (Rajput et al., 2022), it is only active under UV light which is difficult

to harvest as it only constitutes roughly 4 % of the solar spectrum and could potentially be harmful upon overexposure. Visible light makes up approximately 43 % of the solar spectrum and as a result, the quest for visible light sensitive photocatalysts is on the rise (Ichipi et al., 2021). Tungsten trioxide (WO_3) has received considerable attention as a potential photocatalyst since it is easy to synthesize, its structures and stoichiometries are widely tunable, it is highly stable under both basic and acidic environments, it has strong photocatalytic oxidizing ability, it is chemically stable, and has an attractive wide range bandgap of 2.4 – 2.8 eV (Quan et al., 2020). To the best of our knowledge, the photocatalytic degradation of Rhodamine B dye using a crystalline mixture of $\text{WO}_3/\text{WO}_3 \cdot 0.5\text{H}_2\text{O}$ is yet to be reported. This study explores the efficacy of a mixed tungsten oxide-based photocatalyst on the degradation of this dye for the first time.

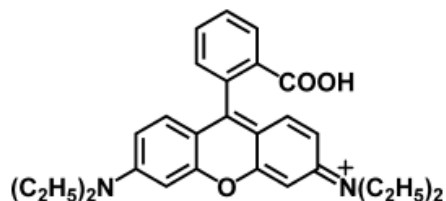


Figure 1: Molecular structure of Rhodamine B

2. Experimental

2.1 Chemicals and reagents

Rhodamine B ≥ 95 wt. % HPLC grade powdered dye and sodium tungstate dihydrate ($\text{Na}_2\text{WO}_3 \cdot 2\text{H}_2\text{O}$) were purchased from Sigma-Aldrich (Johannesburg, South Africa). Hydrochloric acid 30 wt. % - 33 wt. % (HCl), sulphuric acid 98 wt. % (H_2SO_4) and sodium hydroxide pellets (NaOH) were purchased from Glassworld (Johannesburg, South Africa). Deionized water was used throughout this synthesis.

2.2 Synthesis

WO_3 nanoparticles were synthesized using a simple chemical precipitation method at room temperature adopted from Altanany et al. (2018) and modified. A sodium tungstate solution was prepared by dissolving 3 g of sodium tungstate dihydrate in 200 mL of deionized water under continuous stirring for 5 h. The resulting precipitate was allowed to age at room temperature for 24 h. The product was collected and washed several times with distilled water and thereafter oven-dried at 100 °C for 1 h. After which, the product was calcined in a muffle furnace at 300 °C for 4 h.

2.3 Characterization

The crystallinity and composition of the particles was detected using X-ray diffraction (XRD) analysis. The samples were prepared according to the standardized Panalytical backloading system, which provides a nearly random distribution of the particles. The samples were analyzed using a PANalytical X'Pert Pro powder diffractometer in θ - θ configuration with an X'Celerator detector and variable divergence- and fixed receiving slits with Fe filtered $\text{Co-K}\alpha$ radiation ($\lambda=1.789\text{\AA}$). The mineralogy was determined by selecting the best-fitting pattern from the ICSD database to the measured diffraction pattern, using X'Pert Highscore plus software. The particle morphology and elemental analysis and mapping was detected using Zeiss 540 Ultra FEGSEM. The morphology was confirmed using Joel 2100 FEGTEM. Specific surface area analysis was performed using Micromeritics Tristar II 3020 Version 3.02 in liquid nitrogen at 77.350 K. The samples were degassed at 110 °C overnight prior to the specific surface area analysis.

2.4 Photocatalytic activity

Photodegradation studies were carried out in an experimental box of dimensions 0.915 m x 0.705 m lined with aluminum foil to eliminate influence of external light. The box was fitted with 3 x 18 W fluorescent day light lamps. A 5 ppm solution of Rhodamine B was prepared from a 100 ppm stock solution. Before irradiation, varying masses of the photocatalyst ranging from 0.05 g to 1 g were placed in 100 mL of the 5 ppm Rhodamine B solution in a beaker. Preliminary experiments showed that the degradation of Rhodamine B using WO_3 -based particles was highly pH dependent, with rapid degradation occurring under alkaline conditions. An optimum pH of 9.5 was chosen for this study. The pH was adjusted using 0.1 M H_2SO_4 and 0.1 M NaOH. The solution was stirred for 30 min in the dark to reach adsorption-desorption equilibrium. The reaction mixture was continuously homogenized throughout the analysis using a magnetic stirrer. During visible light irradiation, 2 mL samples were collected at 30 min intervals and centrifuged at 10,000 rpm for 5 min. The samples were analyzed using a

WPA, LIGHT Wave, Labotech UV-vis spectrophotometer (South Africa) at a characteristic wavelength of 555 nm using deionized water as a blank. Standard solutions were used to prepare a calibration curve which was used to determine the concentrations of the samples. The tests were conducted in triplicate for statistical purposes. The efficiency of photodegradation was calculated using the expression shown in equation (1):

$$\% \text{ Degradation} = \frac{C_0 - C_t}{C_0} \times 100 \quad (1)$$

Where C_0 is the initial Rhodamine B concentration and C_t is the concentration of Rhodamine B at any given time, t .

3. Results and discussion

3.1 X-ray diffraction (XRD) spectra

Figure 2 shows the XRD spectra of the neat and calcined WO_3 particles. The neat particles were highly amorphous while the particles calcined at 300°C assumed crystallinity. The XRD spectra of the particles calcined at 300°C confirmed the presence of WO_3 . An additional phase, $\text{WO}_3 \cdot 0.5\text{H}_2\text{O}$, commonly known as pyrochlore WO_3 hemihydrate was also detected suggesting that the material was biphasic. The characteristic peaks of WO_3 were found at 2θ values of 12° , 24° , 26.5° , 36° , 62° , 65° , 68.5° and 72° , while those of $\text{WO}_3 \cdot 0.5\text{H}_2\text{O}$ were observed at 32.5° and 42° . The XRD patterns were compared with XRD patterns from the JCPD reference files. The diffraction peaks were in agreement with a monoclinic structure (JCPD=24-0747, space group: P21/n). The diffraction peaks corresponded to (0 2 0), (2 0 0), (1 2 0), (-1 1 2), (1 1 2) (0 2 2), (-2 0 2), (2 2 0), (4 0 0) and (-1 1 4) planes of crystalline WO_3 monoclinic structure. Minor impurities that can be attributed to the tungsten precursor were also detected.

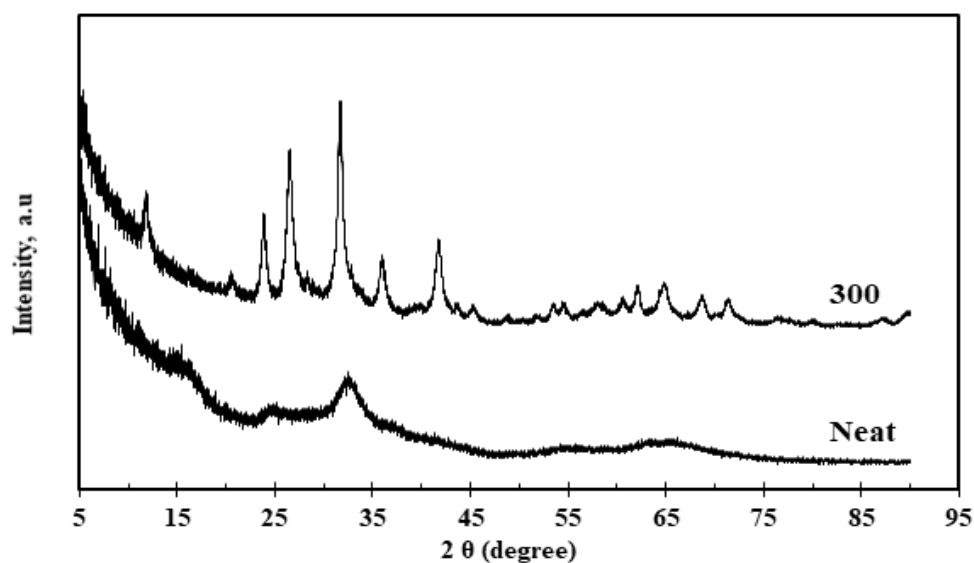


Figure 2: XRD spectra of neat and calcined WO_3 particles

3.2 SEM, TEM and BET analysis

Figure 3a depicts the morphology of the particles calcined at 300°C . It shows an arrangement of agglomerated irregular shaped lumps of particles. This was expected because of the high calcination temperature which led to the aggregation of the primary particles. These observations were similar to those reported by (Periasamy et al., 2019) who prepared the same material using a similar procedure. The nanosized nature of the primary particles was confirmed by TEM analysis which revealed an average particle size of 44 nm (Figure 3b). It is also clear that these particles are irregular-shaped. The BET surface area of the neat and calcined particles was 0.16 and $25.44 \text{ m}^2/\text{g}$. This marks a significant 15,689 % increase in surface area. The marked increase in BET surface area can be attributed to the formation of a porous structure.

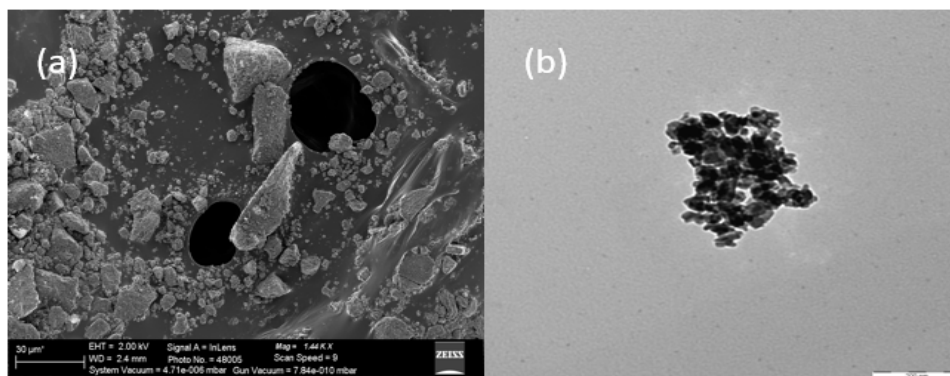


Figure 3: (a) SEM image for calcined WO_3 particles (b) TEM image for calcined WO_3 particles

3.3 SEM/EDS analysis

Figure 4 illustrates the elemental composition of the calcined particles. The EDS spectra depict the presence of W, O, Na and Sb. The atomic percentage of W:O of 24.53:73.97 corresponds to an approximate 1:3 stoichiometric ratio. This confirms that WO_3 was indeed formed. The high percentage of oxygen can be attributed to the presence of oxygen vacancies. Zhao et al. (2018) theorized that the oxygen vacancies in photocatalysts typically act as active sites to improve carrier separation efficiency thus improving the overall photocatalytic activity. At 0.5 keV, a sodium peak is observed which constitutes 1.22 atom % of the total composition. This peak can be attributed to minor impurities from the tungsten precursor. Interestingly, at approximately 3.5 keV, an antimony peak is observed which constitutes 0.28 atom % of the total composition. It is well known that antimony is produced as a by-product of heating certain metals hence this peak could potentially be a result of calcination. There were no peaks for carbon. This indicates the absence of organic compounds.

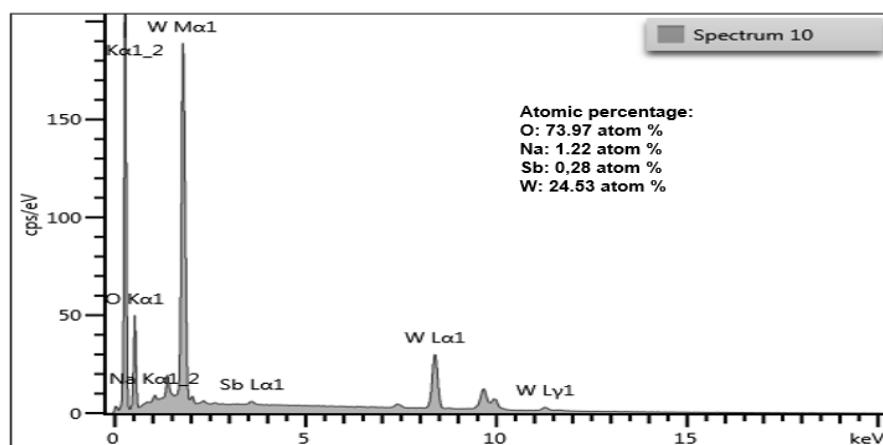


Figure 4: SEM/EDS mapping of calcined WO_3

3.4 Photocatalytic activity

Figure 5 shows the effect of varying the catalyst loading on dye decolorization. No degradation was observed at a catalyst loading of 0.5 g/L. However, degradation was observed as the loading increased to 1 g/L with the maximum degradation of 96.07 % recorded at a loading of 5 g/L. Further addition of the catalyst beyond this loading resulted in a significant decrease in the degradation efficiency. At 10 g/L, the degradation achieved was almost equal to that achieved at a loading of 1 g/L. This drastic decline was attributed to an increase in the turbidity and opacity of the suspension at heightened loadings. As the catalyst loading increased, the number of active sites on the surface of the catalyst decreased resulting in the retardation of the penetration of photons. These obstructed photons were then scattered within the reaction vessel (Gnanaprakasam et al., 2015). The optimum loading of 5 g/L was chosen for further experiments. The degradation of Rhodamine B as a function of irradiation time is shown in Figure 6. The results show that 96.07 % of the Rhodamine B was degraded after 4 h of irradiation under visible light. Blank experiments were performed in the absence of the photocatalyst

(photolysis) and in the absence of light (catalysis/adsorption) while keeping all other reaction conditions constant. No sizable degradation was observed under these conditions. This confirmed that the presence of the photocatalyst and the light source are necessary prerequisites for dye degradation. This remarkable performance can be attributed to the porous nature of the particles and the large surface area which improved the separation and migration efficiency of the photogenerated electron-hole pairs, slowing down charge recombination thereby improving photocatalytic efficiency (Zhang et al., 2014). It is worth noting that photocatalysis is a surface phenomenon and is therefore highly pH dependent. The pH influences the adsorption capacity of the particles and the concentration of the hydroxyl reactive radicals (Azeez et al., 2018). At a pH of 9.5, there is an abundance of hydroxide ions rendering the surface of WO_3 negatively charged. The negatively charged surface of WO_3 has a high affinity for the adsorption of the cationic dye. The positively charged nitrogen as seen in Figure 1 binds to the negatively charged surface of WO_3 resulting in N-demethylation accompanied by the cleavage of the conjugated aromatic rings due to their reaction with the generated hydroxyl free radicals.

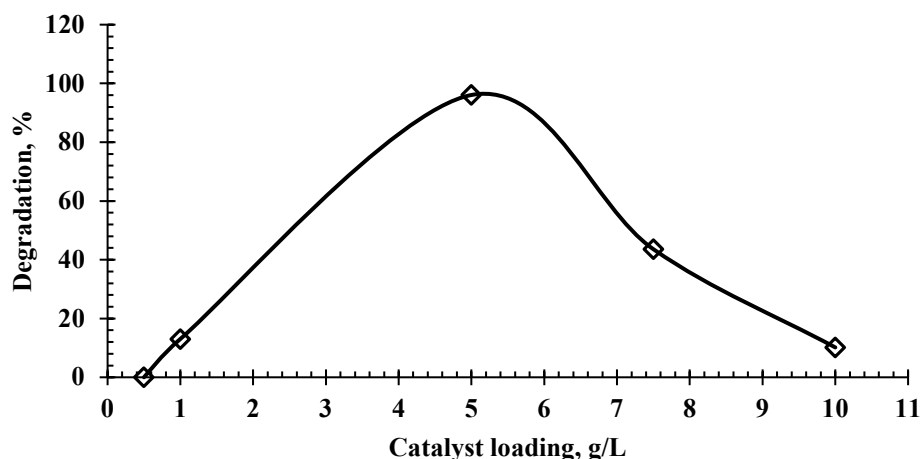


Figure 5: Effect of varying catalyst loading

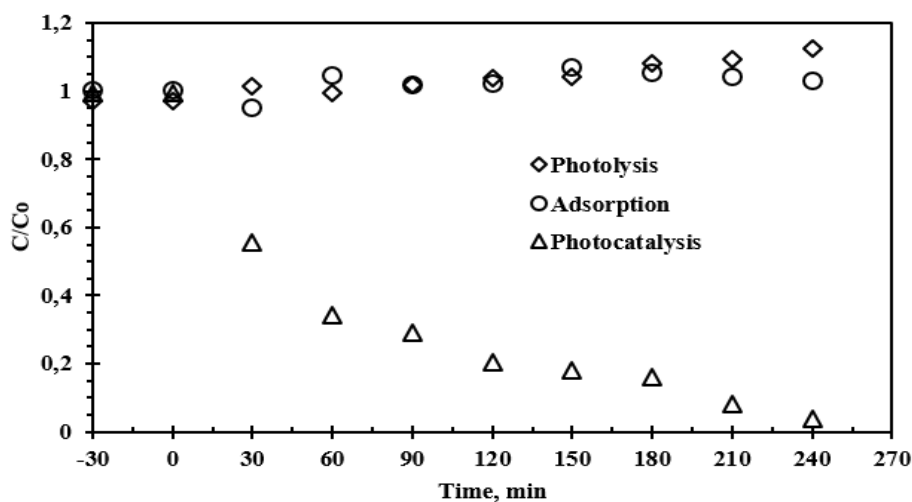


Figure 6: Rhodamine B degradation as a function of time under visible light irradiation

4. Conclusion

Tungsten trioxide (WO_3) particles were synthesized via a simple chemical precipitation method. The efficacy of the photocatalytic degradation of Rhodamine B under visible light irradiation using WO_3 as a catalyst was investigated. A degradation of 96.07% was obtained with no sizable contribution from adsorption and photolysis. Characterization revealed that the synthesized material was biphasic with an arrangement of agglomerated

irregular shaped lump of particles. Calcination of the material resulted in a significant increase in surface area. These physical properties are the driving force behind the remarkable performance of the catalyst. The pH of 9.5 under which the experiments were conducted also played a role in this result. Based on the results obtained, it can be concluded that WO_3 is a potential visible light photocatalyst for the treatment of dye infested wastewater. However, research is still limited to laboratory-scale where simulated visible light is used. Further improvement of the photocatalytic efficiency of WO_3 -based photocatalysts can be investigated by exploiting the tunability of its structure to promote the transfer and separation of photogenerated charge carriers and extend light absorption in the visible region of the spectrum. This can be achieved through phase control, oxygen-vacancy control, active-facet control, morphology control, elemental doping, noble metal loading, hybridization with carbon materials and coupling with other semiconductors. This will potentially reduce the reaction contact time and extend the application to industrial-scale under direct beam solar radiation.

References

- Adenuga D.O., Tichapondwa S.M., Chirwa E.M.N., 2019, Synthesis and characterisation of potential visible-light photocatalyst and its photocatalytic activity in the decomposition of phenol, *Chemical Engineering Transactions*, 74, 1087–1092.
- Altanany S.M., Gondal M.A., Baig U., 2018, Synthesis and characterization of CuO/WO_3 nanocomposite using hybrid method: Simple precipitation and pulsed laser ablation in liquids technique, In: *AIP Conference Proceedings*, American Institute of Physics Inc., AIP Publishing LLC, USA, 2(1), 020014.
- Azeez F., Al-Hetlani E., Arafa M., Abdelmonem Y., Nazeer A.A., Amin M.O., Madkour M., 2018, The effect of surface charge on photocatalytic degradation of methylene blue dye using chargeable titania nanoparticles, *Scientific Reports*, 8, 1-9.
- Gnanaprakasam A., Sivakumar V.M., Thirumarimurugan M., 2015, Influencing Parameters in the Photocatalytic Degradation of Organic Effluent via Nanometal Oxide Catalyst: A Review, *Indian Journal of Materials Science*, 2015, 1–16.
- Ichipi E.O., Tichapondwa S.M., Chirwa E.M.N., 2021, Photocatalytic activity of visible-light-driven ternary $\text{Ag}/\text{Ag}_2\text{S}/\text{ZnO}$ nanocomposites for phenol degradation in water, *Chemical Engineering Transactions*, 86, 817–822.
- Jiang Q., Chen S., Deng X., Feng Y., Reddy N., Zhu Q., Liu W., Qiu Y., 2019, A sustainable low temperature yarn reinforcing process to reduce water and energy consumptions and pollution in the textile industry, *Journal of Cleaner Production*, 210, 646–652.
- Periasamy P., Krishnakumar T., Sandhiya M., Sathish M., Chavali M., Siril P.F., Devarajan V.P., 2019, Electrochemical investigation of hybridized WO_3 - CdS semiconducting nanostructures prepared by microwave-assisted wet chemical route for supercapacitor application, *Journal of Materials Science: Materials in Electronics*, 30, 9231–9244.
- Quan H., Gao Y., Wang W., 2020, Tungsten oxide-based visible light-driven photocatalysts: Crystal and electronic structures and strategies for photocatalytic efficiency enhancement, *Inorganic Chemistry Frontiers*, 7(4), 817-838.
- Rafiq A., Ikram M., Ali S., Niaz F., Khan M., Khan Q., Maqbool M., 2021, Photocatalytic degradation of dyes using semiconductor photocatalysts to clean industrial water pollution, *Journal of Industrial and Engineering Chemistry*, 97, 111-128.
- Rajput R.B., Jamble S.N., Kale R.B., 2022, A review on $\text{TiO}_2/\text{SnO}_2$ heterostructures as a photocatalyst for the degradation of dyes and organic pollutants, *Journal of Environmental Management*, 307, 114533.
- Scarsella M., Bracciale M.P., de Caprariis B., de Filippis P., Petruzzo A., Pronti L., Santarelli M.L., 2017, Improved photocatalytic properties of doped titanium-based nanometric oxides, *Chemical Engineering Transactions*, 60, 133–138.
- Tavakoli-Azar T., Mahjoub A.R., Sadjadi M.S., Farhadyar N., Sadr M.H., 2020, Improving the photocatalytic performance of a perovskite ZnTiO_3 through $\text{ZnTiO}_3@\text{S}$ nanocomposites for degradation of Crystal violet and Rhodamine B pollutants under sunlight, *Inorganic Chemistry Communications*, 119, 108091.
- Yu K., Yang S., He H., Sun C., Gu C., Ju Y., 2009, Visible light-driven photocatalytic degradation of rhodamine B over NaBiO_3 : Pathways and mechanism, *Journal of Physical Chemistry A*, 113(37), 10024–10032.
- Zhang C., Li Y., Shuai D., Shen Y., Wang D., 2019, Progress and challenges in photocatalytic disinfection of waterborne Viruses: A review to fill current knowledge gaps, *Chemical Engineering Journal*, 355, 399-415.
- Zhang M., Xu J., Zong R., Zhu Y., 2014, Enhancement of visible light photocatalytic activities via porous structure of $\text{g-C}_3\text{N}_4$, *Applied Catalysis B: Environmental*, 147, 229–235.
- Zhao S., Zhang Y., Zhou Y., Qiu K., Zhang C., Fang J., Sheng X., 2018, Reactable polyelectrolyte-assisted preparation of flower-like $\text{Ag}/\text{AgCl}/\text{BiOCl}$ composite with enhanced photocatalytic activity, *Journal of Photochemistry and Photobiology A: Chemistry*, 350, 94–102.